01,07

Structure and mechanical properties of layered composites consolidated by high-pressure torsion of amorphous and crystalline aluminum alloy ribbons

© S.V. Vasiliev[1,2], E.A. Sviridova[1,2], A.I. Limanovskii[1], V.M. Tkachenko[1], T.V. Tsvetkov[1], V.V. Burkhovetskii[1], V.N. Varyukhin[1], V.I. Tkatch[1]

[1] A.A. Galkin Donetsk Institute for Physics and Enginireeng, Donetsk, Russia
[2] Donbass National Academy of Civil Engineering and Architecture, Makeyevka, Russia

E-mail: ksvir@list.ru

Received October 30, 2023
Revised October 30, 2023
Accepted October 31, 2023

The structure and mechanical properties of layered composites composed of amorphous $Al_{86}Ni_9Gd_5$ alloy ribbons placed between two crystalline rapidly cooled $Al_{95.8}Mn_{3.8}Fe_{0.4}$ alloy ribbons and consolidated by high-pressure torsion (HPT) were studied by X-ray diffraction analysis, scanning electron microscopy, measurements of microhardness and three-point bending tests. The influence of a high-strength amorphous component on the structure, microhardness and plasticity of the disks consolidated at various degrees of deformation was studied. It was found that by combination of hardness and plasticity, the composite disks synthesized in the work were superior to that of the two layer disks consolidated by the HPT method, consisting of amorphous tapes, and disks composed of amorphous ribbons with aluminum foil coatings. The possible factors causing additional hardening of composite disks were discussed.

Keywords: layered composites, high-pressure torsion, rapidly cooled ribbons, amorphous and crystalline structure, consolidation, hardness, plasticity.

DOI: 10.61011/PSS.2023.12.57685.223

1. Introduction

Aluminum-based alloys are a class of structural materials that, due to their high specific strength and corrosion resistance, play an important role in aviation and space engineering, therefore the increase of the level of their mechanical properties has been an urgent task for many decades. The implementation of the known hardening mechanisms (solid solution, grain boundary, stress (dislocation) and precipitation (of second-phase particle), considered for Al alloys in the paper [1], led to the creation of commercial alloys with a tensile strength $\leq 650-700$ MPa [2,3]. The processing of aluminum alloys using modern methods of severe plastic deformation (SPD) made it possible to form structures with a combination of several strengthening mechanisms, which made it possible to increase their strength. In particular, in samples of a high-strength commercial 7075 Al alloy with nanoscale microstructure elements formed by high-pressure torsion (HPT), a yield strength of 1 MPa was achieved in combination with the plasticity of 5% [3].

Promising developments to increase the strength of aluminum alloys include the formation of thermodynamically non-equilibrium crystalline and amorphous structures by quenching from a liquid state. In particular, in the bulk samples obtained by extrusion of rapidly cooled alloy granules based on the system Al–Zn–Mg, the tensile strength over 0.8 GPa was achieved [4]. Even higher levels of strength were found in amorphous aluminum alloys alloyed with rare earth metals (REM) and transition metals (TM) (up to 1.0–1.2 GPa), and in amorphous-nanocrystalline composites, the tensile strength of which can reach 1.56 GPa [5,6]. However, the main obstacle to the practical use of aluminum alloys with an amorphous and nanocomposite structure is the low glass-forming tendency of melts, as a result of which the maximum size of amorphous samples achieved to date (at least in one dimension) does not exceed 2.5 mm [7], therefore, the vast majority of Al-REM-TM glasses are obtained in the form of ribbons, flakes or powders with sizes which not exceed than 100 μm.

To overcome this obstacle the consolidation of rapidly cooled materials is necessary, however, the temperature conditions of this process in the traditional methods of powder metallurgy such as hot pressing and extrusion lead to the complete decomposition of nonequilibrium states and, accordingly, degradation of mechanical properties [4,5]. To solve this problem, SPD methods turned out to be more effective [8], in which, due to plastic flow, complete consolidation of dispersed materials is achieved at significantly lower temperatures, which makes it possible to fully or partially retain nonequilibrium structural states and an increased level of strength properties [9,10].

Moreover, as recent experiments have shown [11], the nanocomposite structure formed during the consolidation of

the amorphous ribbons $Al_{86}Ni_9Gd_5$ by HPT, has, together with higher hardness, also increased ductility compared to a similar structure formed during the heating process. This is, of course, an important practical effect of SPD, which is due to the creation of an increased concentration of free volume in the amorphous phase during deformation [12]. Taking into account that high-strength samples with amorphous and nanocomposite structures have relatively low ductility (usually $\leq 2\%$), the level increasing of this characteristic is an urgent task.

As noted in the paper [13], the plasticity of amorphous alloys increases under conditions of deformation in constrained volumes, which leads to the formation of multiple shear bands. Such conditions are created, in particular, during the deformation of layered structures composed of materials with different mechanical properties (for example, soft glasses based on La and hard glasses based on Zr) [14]. Another way to increase the ductility of metallic glass samples is application of coatings that reduce the concentration of surface defects [15]. Recent studies [16] have also shown that coatings have a beneficial effect on the plasticity of samples obtained by consolidating amorphous ribbons using the HPT method. In particular, the plasticity of a package consisting of two amorphous ribbons of the $Al_{86}Ni_9Gd_5$ alloy, placed between foils of pure Al and consolidated by HPT method, was 3.6%, which is by 2.5 times higher than the plasticity of the uncoated package.

Considering these results, it seems appropriate to carry out the similar experiments, but with two nonequilibrium materials to use the crystalline rapidly cooled ribbons of the $Al_{95.8}Mn_{3.8}Fe_{0.4}$ alloy, two-layer samples of which, consolidated by HPT method have a significantly higher hardness compared to foils of pure Al in combination with relatively high plasticity (3.0–4.7%) [17] as a coating for the two layer two-layer package of amorphous ribbons $Al_{86}Ni_9Gd_5$.

2. Materials and experimental procedure

As the initial materials for the production of layered composites the ribbons 10 mm wide of $Al_{95.8}Mn_{3.8}Fe_{0.4}$ (AlMnFe) alloy $55 \pm 5\,\mu$m thick, and of $Al_{86}Ni_9Gd_5$ (AlNiGd) alloy $65 \pm 5\,\mu$m thick were used, which were produced by melt spinning in air and in He atmosphere respectively. Previous studies [17] showed that the first of these ribbons had a crystalline structure (FCC Al-based solid solution), while the second one was amorphous. Layered samples were prepared by placing a double-folded piece of amorphous ribbon inside a double-folded crystalline ribbon and spot welding of the free ends of the package together. Such formed packages formed in this way with dimensions of about $10 \times 10 \times 0.25$ mm were placed between flat anvils with a diameter of 5 mm and deformed by rotating through $N = 1$, 2 and 4 turns under a pressure of 2 GPa. After deformation the excess material was removed, and the consolidated samples with diameter of 5 mm and 169, 168 and 165 (± 5) μm thick had a slightly convex shape, typical for this type of deformation [18].

The mechanical properties of the consolidated samples were studied by microhardness measurements and three-point bending tests. Microhardness (H_μ) was measured on a standard hardness tester PMT-3 under a load of 0.49 N for 10 s along the diameter of the disks approximately after every 0.25 mm. H_μ values measured on three samples treated according to the same scheme were averaged and used as a characteristic. Due to the inhomogeneous structure of the samples and surface roughness, the scatter of the measurement results was 10–15%.

Testing of disks for three-point bending was carried out on a homemade setup mounted on the base of an instrumental microscope MMI-2, with spanning distance L of 2.01 ± 0.005 mm. The loading nose is rigidly connected to one of the ends of the strain gauge beam. The other end of the beam is connected to the movable measuring table of the microscope. The microscope table is moved using micrometer screws with an accuracy of at least 5 μm. The magnitude of the loading force is measured using the strain gauge beam designed for load of up to 9.8 N and calibrated by the weight method to this load with the increments of 0.5 N. The conversion coefficient was obtained using the linear regression method, which ensured the accuracy of measuring the magnitude of the applied force was not lower than $\pm 10^{-2}$ N. The sample was loaded at a stepwise mode with increment 10 μm with an average rate of 0.1 mm/min.

Based on the experimentally measured strain diagrams in accordance with the requirements of GOST R 56810–2015 (ASTM standard D 790–10), the following characteristics were calculated:

– sample fracture stress

$$\sigma_{\mathrm{m}} = \frac{3FL}{2bd^2} \tag{1a}$$

(for „thick“ samnples, $L \leq 16d$) and

$$\sigma_{\mathrm{m}} = \frac{3FL}{2bd^2}\left[1 + 6\left(\frac{\delta}{L}\right)^2 - 4\left(\frac{\delta d}{L^2}\right)\right] \tag{1b}$$

for „thin“ samples;

– strain on the external surface of sample

$$\varepsilon = \frac{6\delta d}{L^2} \tag{2}$$

and modulus of elasticity in bending

$$E_b = \frac{mL^3}{4bd^3}, \tag{3}$$

where F is the applied force, L is the spanning distance, b and d are the width (disk diameter) and thickness respectively, δ is the deflection of the sample center, m is the slope of the initial straight-line portion of the load-deflection curve. Tests were carried out on at least three samples, followed by averaging of the measurement results.

The morphological features of the structure of the consolidated disks were studied by scanning electron microscopy

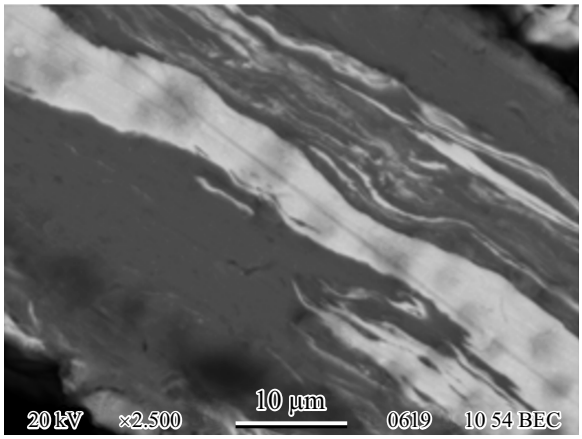

Figure 1. Microstructure of the section (at a distance ~ 1.5 mm from the center) of a 4-layer disc (2 layers of an amorphous ribbon (light) between layers of a crystalline ribbon (dark)), deformed according to the mode 2 turns under pressure 2 GPa.

(JSM-6490LV microscope). The outer surfaces of the samples and the fracture surfaces, as well as the internal structure, were studied. Changes in the phase composition of the samples caused by deformation were studied by X-ray analysis (DRON-3M diffractometer).

3. Results and discussion

Microstructural studies of consolidated composite samples showed that almost complete consolidation of amorphous ribbons with each other and with crystalline ribbons occurs after rotation by 2 turns under pressure of 2 GPa (Figure 1), while samples deformed by $N = 1$ during bending tests delaminated [19]. X-ray studies of the consolidated four-layer composite disks (Figure 2) showed that only the lines of FCC Al-based solid solution are present in the diffraction patterns. This is a completely expected result, since the amorphous ribbons are located inside a shell of crystalline layers (Figure 1), and the deformation even by $N = 4$ turns out to be insufficient for a significant movement of the amorphous material into the outer layers of the disks.

Analysis of the diffraction patterns shown in Figure 2 showed that increase in the degree of deformation leads to a slight increase in the width of the reflection (111), which, according to the Selyakov–Scherrer relation [20], corresponds to a decrease in the size of the coherent scattering regions (c.s.s.) from 42 to 38 nm. The lattice constant in these disks, calculated from line (400), remains unchanged and equals to 0.4032 ± 0.0001 nm, which is slightly lower than the lattice constant of pure Al (0.4049 nm [20]). This value coincides with the lattice constant of the undeformed AlMnFe ribbon [21] and means that the solid solution formed in the ribbon during melt quenching is retained during deformation. At the same time c.s.s. of Al of the solid solution in composite disks is lower compared to the size in two-layer deformed disks (49–58 nm), which may be due to the influence of the amorphous phase.

The influence (contribution) of the amorphous ribbon is more clearly manifested in changes in the microhardness of the surface of composite disks, measured along the diameters (Figure 3, 4). As can be seen from the data presented, the microhardness values are distributed symmetrically relative to the disc center, which is typical for samples deformed by this method, since the degree of deformation is proportional to the distance from the center.

The microhardness values of two-layer disks made of AlMnFe and AlNiGd alloys, deformed at 2 GPa $N = 1$mode lie within the ranges of 1.87–2.12 GPa and 3.17–4.12 GPa, respectively, i. e. the hardness of even the central part of the samples is higher than H_μ of the initial ribbons (Figure 3). At the same time, despite the fact that the amorphous ribbon is located inside the composite disks, the hardness of their peripheral regions turned out to be significantly higher, and of the central zone was lower than the hardness values of the disks made of crystalline ribbon (Figure 3).

In four-layer packages, depending on the degree of deformation, the microhardness changed as follows (Figure 4): after one turn it was within the range of 1.33–3.81 GPa, after 2 turns — 1.69–4.12 GPa and after 4 turns — 1.69–4.87 GPa. Thus, the presence of the amorphous ribbon is manifested not only in the microhardness decrease in the central part of the disc from 1.87 to 1.33 GPa, but also in increase in its periphery from 2.12 to 4.87 GPa.

To assess the strength characteristics of disks with heterogeneous structure, consolidated by the HPT method,

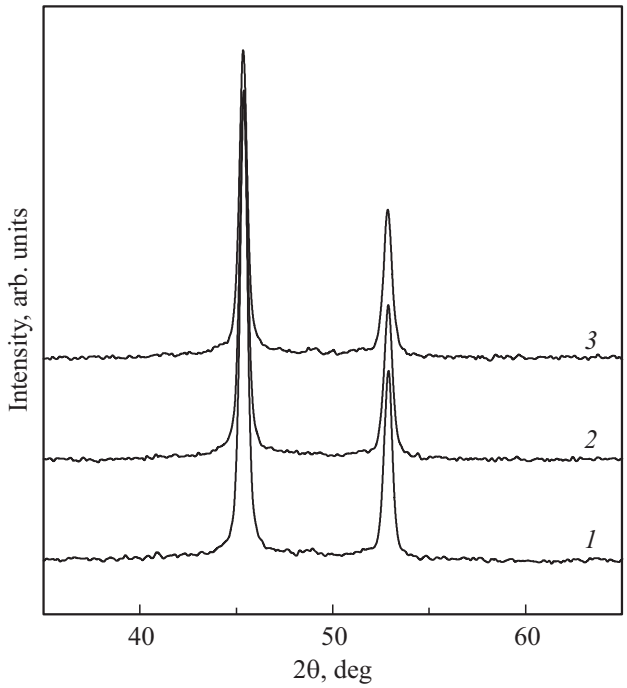

Figure 2. Diffraction patterns of the surface of 4-layer composite disks consolidated under the pressure of 2 GPa with different degrees of strain N: *1* — 1, *2* — 2 and *3* — 4 turns.

and compare them with the structure, it seemed appropriate to determine the average microhardness values. Estimates carried out for the dependences $H_\mu(r)$ in Figure 4 showed that the average microhardness of the composite disc deformed by one turn is 2.86 ± 0.96 GPa and increases almost linearly with increasing the degree of plastic deformation to

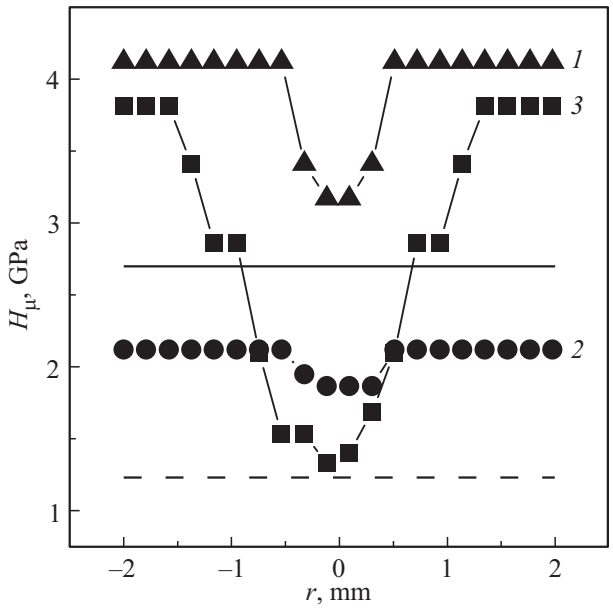

Figure 3. Microhardness of the surface of layered disks (*1* — two layers of amorphous ribbon AlNiGd, *2* — two layers of crystalline ribbon AlMnFe and *3* — 4-layer composite), consolidated according at the 2 GPa/1 turn mode. The dashed and solid lines show H_μ of the initial ribbons AlMnFe and AlNiGd, respectively.

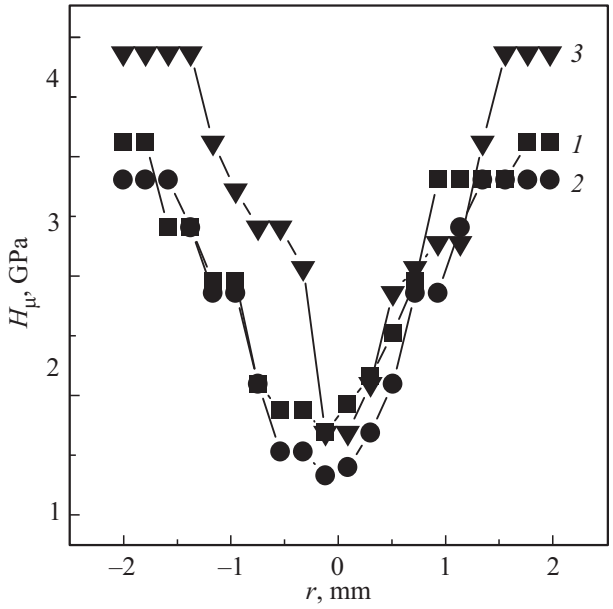

Figure 4. Influence of the degree of deformation under pressure 2 GPa (*1* — 1 turn, *2* — 2 turns and *3* — 4 turns) on the microhardness of the surface of 4-layer disks.

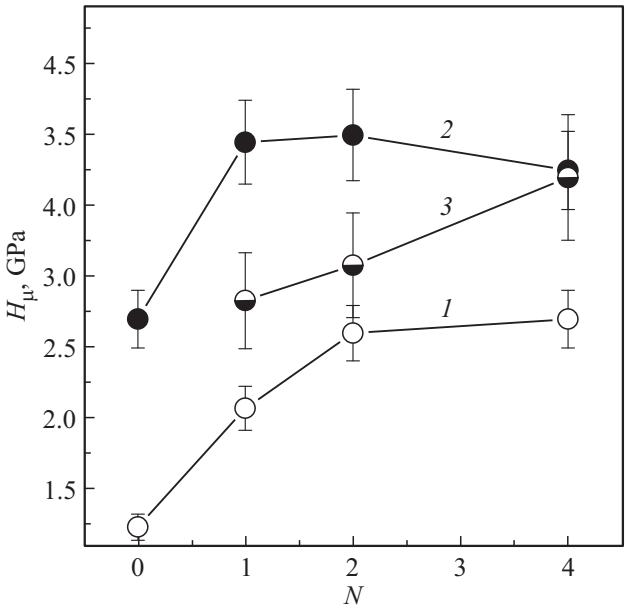

Figure 5. The influence of the degree of deformation on the average microhardness of consolidated disks: *1, 2* — two-layer with a crystalline [17] and amorphous [22] structure, respectively, *3* — four-layer.

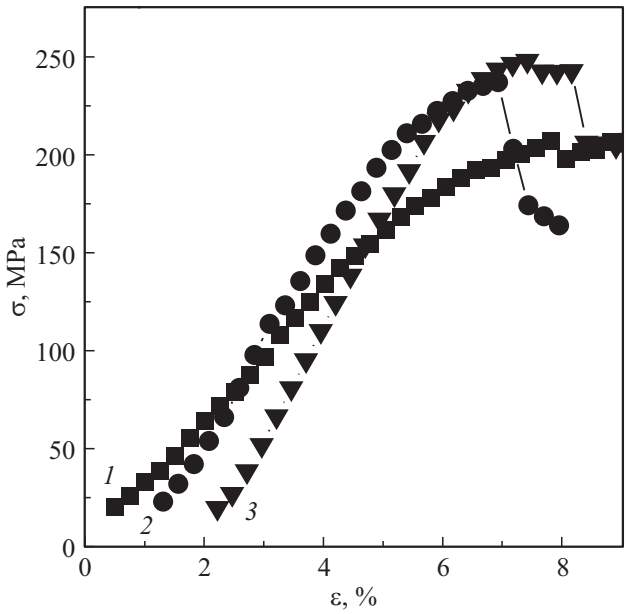

Figure 6. Typical curves „stress–strain" 4-layer composite disks consolidated under pressure of 2 GPa with different degrees of strain: *1* — 1 turn, *2* — 2 turns and *3* — 4 turns.

3.70 ± 1.1 GPa (Figure 5). It seemed interesting to compare this dependence with the changes $H_\mu(N)$ of two-layer disks consisting of ribbons of AlNiGd and AlMnFe alloys, which are given in the papers [22] and [17], respectively. From a comparison of these data (Figure 5) it follows that the hardness of two-layer disks, consolidated from crystalline and amorphous ribbons, increases along curves

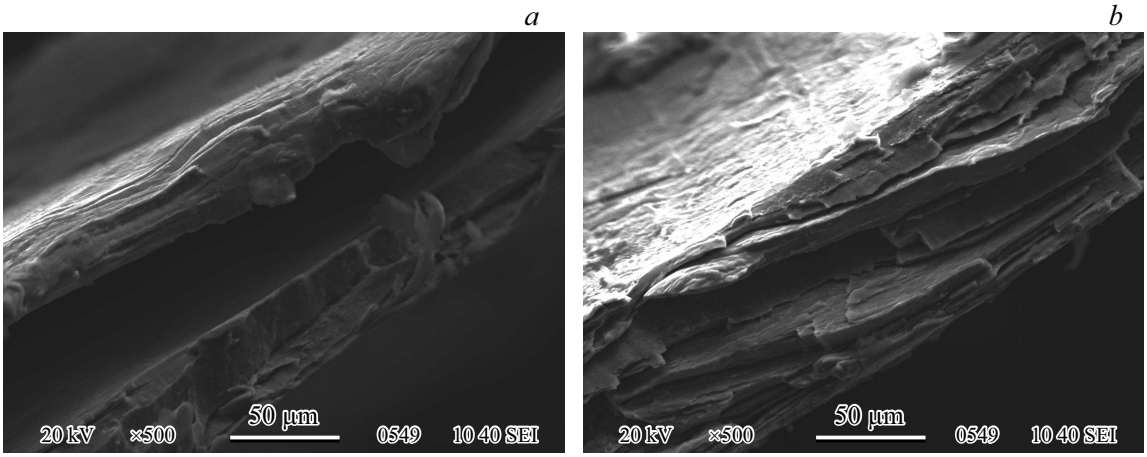

Figure 7. SEM micrographs of the fracture surface of four-layer disks deformed by rotation by 1 (a) turn and 4 (b) turns.

with saturation (from 1.23 to 2.7 GPa and from 2.7 to 3.75 GPa) and, thus the average hardness of the composite disks composed of amorphous and crystalline ribbons and consolidated by torsion by $N = 4$ is compared with the hardness of two-layer disc consisting of amorphous ribbons. Note that the similar result (the same H_μ) was observed for consolidated disks consisting of crystalline ribbon between two amorphous ribbons of AlNiGd alloy [22]. Moreover, as established in the paper [23] the hardness of the composite sample consolidated from two amorphous ribbons of alloys $Fe_{53.3}Ni_{26.5}B_{20.2}$ and $Co_{28.2}Fe_{38.9}Cr_{15.4}Si_{0.3}B_{17.2}$, in a certain range of deformations was higher than each of the components). For the composite consisting of two amorphous ribbons on an iron-nickel and iron-cobalt base, this result was explained by the probable formation of additional intermetallic phases at the interfaces. However, considering the low content of manganese and iron in the AlMnFe alloy, the formation of intermetallic compounds with these metals at the interface with the AlGdNi ribbon seems unlikely.

On the other hand, the composite material (the amorphous ribbon between crystalline ribbons) studied in this paper and the composite in the paper [22] (a crystalline ribbon of similar composition between amorphous ribbons) with a hardness equal to the hardness of the amorphous ribbon have a common characteristic structural feature — the presence of vortex-like mixing of materials of amorphous and crystalline ribbons in the middle zone of deformed disks (Figure 1). The instabilities of flow of this kind arise at certain levels of joint inhomogeneous plastic deformation of layered samples made of materials with different strength characteristics [24,25]. Analysis [25] showed that after the pressure removal in this zone of the sample stresses of the second kind are created: compressive stresses in a softer material and tensile stresses in harder material. Since the hardness of the amorphous AlGdNi alloy is by more than two time exceeds the hardness of the crystalline alloy, the increased values H_μ of the composite sample are most likely associated with the contribution of additional microstresses in the AlMnFe alloy. Also one do not exclude the possible contribution to sample strengthening from the enrichment of grain boundaries [1] of the AlMnFe alloy with Ni and Gd atoms from the amorphous phase, caused by deformation-stimulated diffusion.

As it is known [26], the strength characteristics of metal alloys: hardness and tensile strength are related to each other by the approximate relation $H \approx 3\sigma_b$ and, consequently, the microhardness values of deformed disks at the level 3−4 GPa correspond to the tensile strength 1−1.33 GPa, significantly exceeding the characteristics of commercial high-strength Al-based alloys. Plasticity is another equally important property of structural materials. To evaluate this characteristic of consolidated disks, three-point bending tests were carried out, the results of which are shown in Figure 6.

Experimental curves „load−deformation“ of composite disks have a typical shape for this type of test, indicating the presence of elastic deformation (linear sections) and plastic deformation. Processing of test results showed that the increase in the degree of strain (from one turn to four turns) leads to the increase in the fracture load from 207 ± 20 MPa to 240 ± 20 MPa and non-monotonic changes in the elastic modulus during bending (3.4, 6.0 and 5.5 (±0.2) GPa) and ductility (3.3, 3.6 and 2.0 (±0.25)%). The values of σ_m and E_b of consolidated 4-layer disks estimated from bending tests are close to the similar characteristics of two-layer disks consisting of amorphous ribbons $Al_{86}Ni_9Gd_5$ (361−368 MPa and 8.5−8.8 GPa) [11], however they are significantly lower than the property ranges of heat-treated ribbons of the same composition (400−1900 MPa and 50−180 GPa) [27]. Apparently, the noted differences are due to reduced adhesion of layers in the central parts of the consolidated disks.

As the analysis of the results of similar tests [27] has shown, the values of E_b and σ_m can only be used as comparative characteristics for samples of the same shape, while the ductility values consolidated disks are less

sensitive to the shape and size of the samples, and are close to those measured by other methods.

The presence of plastic deformation of the consolidated 4-layer disks is confirmed by the results of fractographic studies of samples subjected to three-point bending tests (Figure 7). As can be seen in the SEM images, on the fracture surfaces there are areas with a smooth fracture surface, which is characteristic of the brittle fracture, and with a wavy (vein-like) morphology, corresponding to the ductile type of fracture.

Thus, the results of the studies show that the composite material consolidated by the HPT method, consisting of amorphous ribbon of AlNiGd alloy placed between AlMnFe alloy ribbons, has an average hardness 2.8−3.7 GPa in combination with plasticity 2−3.6%, which is noticeably higher than the plasticity of two-layer disks ($1.4 \pm 0.2\%$), consolidated from two amorphous ribbons [27]. Apparently, the increased plasticity of the hybrid material compared to the deformed amorphous material is due to the presence of crystalline shell (Figure 1), which limits the distribution of shear bands in the amorphous material and promotes their formation.

Note that the level of plasticity of the four-layer disks studied in this paper coincides with the plasticity ($3.6 \pm 0.3\%$) of consolidated disks, in which amorphous ribbons were located between layers of pure aluminum foil [16]. However, the aluminum-coated disks had lower average microhardness (1.95 ± 1.0 GPa), indicating the prospects of developing consolidated hybrid materials using ductile crystalline alloys as shells for high-strength amorphous ribbons.

4. Conclusions

1. It was established that rotation by 2 turns under pressure of 2 GPa leads to almost complete consolidation of the firstly obtained four-layer disks with diameter of 5 mm, consisting of two ribbons of the alloy $Al_{86}Ni_9Gd_5$ with amorphous structure, placed between crystalline alloy ribbons $Al_{95.8}Mn_{3.8}Fe_{0.4}$.

2. It was found that in the central parts of consolidated disks the amorphous ribbon is located in the internal layers, and the increase of its influence with deformation is manifested in increase in the microhardness of the peripheral areas.

3. It was shown that with increase in degree of deformation, the average microhardness of the composite disks increases almost linearly in samples deformed by 1 turn and 2 turns, it is between the values H_μ of disks consisting of amorphous and crystalline ribbons, and at $N = 4$ it is compared with the hardness of disks made of amorphous ribbons.

4. Comparative analysis showed that in terms of the combination of mechanical properties (average microhardness 3.7 GPa and plasticity 3.6%), the composite disks consolidated at $N = 4$ are superior to that of the two-layer disks consisting of amorphous ribbons ($H_\mu = 3.75$ GPa, $\varepsilon_{pl} = 1.4\%$), and composite disks consisting of two amorphous ribbons covered with aluminum foil ($H_\mu = 1.95$ GPa, $\varepsilon_{pl} = 3.6\%$).

5. The same average values of microhardness of disks consolidated at $N = 4$, consisting of hard amorphous ribbons, and four-layer disks containing softer crystalline ribbons are due to the phenomenon of vortex-like mixing of the ribbon materials, which probably may result in additional microstresses or enrichment of the grain boundaries of the AlMnFe crystalline alloy with Ni and Gd atoms, caused by deformation-stimulated diffusion.

Conflict of interest

The authors declare that they have no conflict of interest.

References

[1] T.S. Orlova, D.I. Sadykov, M.Yu. Murashkin, V.U. Kazykhanov, N.A. Enikeev. FTT **63**, *10*, 1572 (2021). (in Russian).
[2] H. Jones. Aluminium **54**, *4*, 274 (1978).
[3] P.V. Liddicoat, X.-Zh. Liao, Y. Zhao, Y. Zhu, M.Y. Murashkin, E.J. Lavernia, R.Z. Valiev, S.P. Ringer. Nature Commun. **1**, 63 (2010).
[4] V.I. Dobatkin, V.I. Elagin, V.M. Fedorov. Bystrokristallizovannye alyuminievaye splavy. VILS, M. (1995). 341 s. (in Russian).
[5] A. Inoue. Prog. Mater. Sci. **43**, 365 (1998).
[6] A. Inoue, H. Kimura. Mater. Sci. Eng. A **286**, 1 (2000).
[7] B.J. Yang, W.Y. Lu, J.L. Zhang, J.Q. Wang, E. Ma. Sci. Rep. **7**, 11053 (2017).
[8] R.Z. Valiev, R.K. Islamgaliev, I.V. Alexandrov. Progr. Mater. Sci. **45**, 103 (2000).
[9] A.R. Yavari, W.J. Botta Fihlo, C.A.D. Rodrigues, C. Cardoso, R.Z. Valiev. Scripta Mater. **46**, 711 (2002).
[10] A.P. Shpak, V.N. Varyukhin, V.I. Tkatch, V.V. Maslov, Y.Y. Beygelzimer, S.G. Synkov, V.K. Nosenko, S.G. Rassolov. Mater. Sci. Eng. A **425**, 172 (2006).
[11] S.V. Vasiliev, A.I. Limanovskii, V.M. Tkachenko, T.V. Tsvetkov, K.A. Svyrydova, V.V. Burkhovetskii, V.N. Sayapin, O.A. Naumchuk, A.S. Aronin, V.I. Tkatch. Mater. Sci. Eng. A **850**, 143420 (2022).
[12] D.V. Gunderov, E.V. Boltynjuk, V.D. Sitdikov, G.E. Abrosimova, A.A. Churakova, A.R. Kilmametov, R.Z. Valiev. IOP Conf. Ser.: J. Phys.: Conf. Ser. **1134**, 012010 (2018).
[13] P. Rizzi, A. Habib, A. Castellero, L. Battezzati. J. Alloys Compds. **509S**, S275 (2011).
[14] P. Sharma, K. Yubuta, H. Kimura, A. Inoue. Phys. Rev. B **80**, 024106 (2009).
[15] J.P. Chu, J.E. Greene, J.S.C. Jang, J.C. Huang, Y.-L. Shen, P.K. Liaw, Y. Yokoyama, A. Inoue, T.G. Nieh. Acta Mater. **60**, 3226 (2012).
[16] S.V. Vasiliev, A.I. Limanovskii, V.M. Tkachenko, T.V. Tsvetkov, K.A. Svyrydova, V.V. Burkhovetskii, V.I. Tkatch. Mater. Lett. **318**, 132155 (2022).

[17] E.A. Sviridova, T.V. Tsvetkov, V.M. Tkachenko, A.I. Limanovskii, V.N. Sayapin, S.V. Vasiliev, V.I. Tkatch. Tr. of the Kola Science Centre of RAS. Ser. Eng. Sci. **13**, *1*, 223 (2022). (in Russian).
[18] I.V. Alexandrov, Y.T. Zhu, T.C. Lowe, R.K. Islamgaliev, R.Z. Valiev. Nanostruct. Mater. **10**, *1*, 45 (1998).
[19] A.I. Limanovskii, V.N. Sayapin, V.M. Tkachenko, E.A. Sviridova, V.I. Parfeniy, S.V. Vasiliev, S.V. Terekhov, V.I. Tkatch. Fizika i tekhnika vysokikh davlenij, **29**, *2*, 5 (2019). (in Russian).
[20] S.S. Gorelik, Yu.A. Skakov, L.N. Rastorguev. Rentgenograficheskiy i elektronno-opticheskiy analiz. MISIS, M., (2002). 360 s. (in Russian).
[21] E.A. Sviridova, T.I. Tsvetkov, V.M. Tkachenko, A.I. Limanovskii, V.I. Sayapin, S.V. Vasiliev, V.I. Tkatch. Tr. of the Kola Science Centre of RAS. Chemistry and Materials **11**, *2*, 219 (2021). (in Russian).
[22] S.V. Vasiliev, A.I. Limanovskii, V.M. Tkachenko, T.V. Tsvetkov, K.A. Svyrydova, V.V. Burkhovetskii, V.N. Sayapin, S.V. Terekhov, V.I. Tkatch. Mater. Today Commun. **24**, 101080 (2020).
[23] I.E. Permyakova, A.M. Glezer, A.I. Kovalev, V.O. Vakhrushev. Pis'ma v ZhETF **113**, *7*, 468 (2021). (in Russian).
[24] R. Kulagin, Y. Beygelzimer, Yu. Ivanisenko, A. Mazilkin, B. Straumal, H. Hahn. Mater. Lett. **222**, 172 (2018).
[25] V. Tavakkoli, A. Mazilkin, T. Scherer, M. Mail, Y. Beygelzimer, B. Baretzky, Y. Estrin, R. Kulagin. Mater. Lett. **302**, 130378 (2021).
[26] P. Zhang, S.X. Li, Z.F. Zhang. Mater. Sci. Eng. A **529**, 62 (2011).
[27] S.V. Vasiliev, T.V. Tsvetkov, K.A. Svyrydova, V.M. Tkachenko, A.S. Aronin, V.I. Tkatch. J. Non-Cryst. Solids **699**, 121968 (2023).

Translated by I.Mazurov